

PAPER • OPEN ACCESS

## Lateral scale calibration for focus variation microscopy

To cite this article: Anas Alburayt *et al* 2018 *Meas. Sci. Technol.* **29** 065012

View the [article online](#) for updates and enhancements.

### You may also like

- [Metrological characteristics for the calibration of surface topography measuring instruments: a review](#)  
Richard Leach, Han Haitjema, Rong Su et al.
- [Comparison of the contact and focus variation measurement methods in the process of surface topography evaluation of additively manufactured models with different geometry complexity](#)  
Anna Bazan, Pawe Turek and ukasz Przeszowski
- [Optical system for the measurement of the surface topography of additively manufactured parts](#)  
Narcis Vilar, Roger Artigas, Carlos Bermudez et al.

# Lateral scale calibration for focus variation microscopy

Anas Alburayt, Wahyudin P Syam  and Richard Leach

Manufacturing Metrology Team, University of Nottingham, NG8 1BB, Nottingham, United Kingdom

E-mail: [wahyudin.syam@nottingham.ac.uk](mailto:wahyudin.syam@nottingham.ac.uk)

Received 31 January 2018, revised 13 March 2018

Accepted for publication 23 March 2018

Published 4 May 2018



## Abstract

Areal surface texture measuring instruments can be calibrated by determining a set of metrological characteristics currently in the final stages of standardisation. In this paper, amplification, linearity and perpendicularity characteristics have been determined to calibrate the lateral performance of a focus variation microscope. The paper presents a novel and low-cost material measure and procedures that are used to determine the characteristics. The material measure is made of stainless steel with a cross-grating grid of hemispherical grooves. The design, manufacture and calibration of the material measure are discussed. The  $20 \times 20$  mm grid is measured with and without image stitching. The results show that the proposed material measure and procedures can be used to determine the error of the amplification, linearity and perpendicularity characteristics. In addition, the lateral stage error can be significantly reduced by measurement with image stitching.

Keywords: metrological characteristics, focus variation microscopy, amplification coefficient, linearity deviation, perpendicularity deviation, lateral calibration

(Some figures may appear in colour only in the online journal)

## 1. Introduction

Areal surface topography measuring instruments are used to characterise functional surfaces with both stochastic and deterministic features [1]. Calibration of the instruments is important to maintain the traceability of their measurement results. The draft international standard ISO/DIS 25178 part 600 [2, 3] recommends the determination of a series of defined metrological characteristics (MCs) to calibrate surface topography instruments. These MCs can be used for calibration of all types of surface topography instruments that use the areal topography configuration defined in ISO 25178 part 6 [4]. By using the defined MCs, different surface topography instruments can be quantitatively compared [3] and specified. Methods for determining the MCs were developed in ISO Technical Committee 213 Working Group 16 and early work was published by the National Physical Laboratory [5–7]

for contact stylus instruments, imaging confocal microscopy and coherence scanning interferometry. MCs are defined in ISO/DIS 25178 part 600 as ‘characteristics of measuring equipment which may influence the results of the measurement’. This definition highlights the importance of MCs, which can contribute immediately to the measurement uncertainty [2, 8]. The MCs for areal surface topography instruments include: measurement noise, flatness deviation, amplification coefficient, linearity deviation,  $x$ - $y$  perpendicularity deviation, topographic spatial resolution and topography fidelity [2, 3]. These MCs can be applied to all non-contact (optical) surface topography instruments that measure surface topography directly, including focus variation microscopy (FVM), but not those that measure statistical parameters of a surface (i.e. use the area-integrating method) [1].

FVM is an areal measurement technique [1, 9] that operates using optical microscope optics with a limited depth of focus objective lens. FVM reconstructs a surface by detecting the height at each position along the surface based on the sharpness of a surface image from an image-stack captured during a scan through focus in  $z$ -direction. The sharpness at a pixel is

 Original content from this work may be used under the terms of the [Creative Commons Attribution 3.0 licence](https://creativecommons.org/licenses/by/3.0/). Any further distribution of this work must maintain attribution to the author(s) and the title of the work, journal citation and DOI.

calculated with respect to their pre-defined neighbour pixels. However, FVM has difficulty when measuring surfaces that are highly reflective and have a lack of texture (approximately with  $R_a$  less than 10 nm but this value is objective dependent) or other contrast-producing phenomena [10–12]. With such surfaces, it is difficult to calculate the sharpness (contrast) for each pixel, corresponding to a specific spatial location on a measured surface with respect to its neighbouring pixels. The calculated sharpness value will be too small to determine the height position with the largest sharpness value within the image stack. A replica method is commonly used with smooth and texture-lacking surfaces with FVM [10, 13], where the replica effectively provides the contrast mechanism.

The MCs are determined using material measures and procedures which are currently still under debate in the ISO working group [14]. According to the default procedures under development, each MC is determined using specified material measures, such as using an optical flat for measurement noise and flatness deviation, and a cross-grating for the amplification, linearity and  $x$ - $y$  perpendicularity [3]. However, there is still a lack of suitable material measures that can be used to determine the MCs for FVM, because most commercial material measures have smooth surfaces. Hence, new material measures for FVM need to be designed, manufactured and calibrated.

This paper will present a novel and low-cost material measure and procedures to determine the amplification coefficient, linearity deviation and  $x$ - $y$  perpendicularity deviation for a FVM. The determination of the measurement noise and flatness deviation for FVM is discussed elsewhere [15]. Two measurement methods (with and without image stitching) have been considered for the calibration of the lateral capability. The second section presents the design, manufacture and calibration of the material measures and the third section details the procedures to determine, and the results for, the amplification coefficient, linearity deviation and perpendicularity deviation. Finally, the fourth section presents the conclusions and future work.

## 2. Material measure and procedures

### 2.1. Material measure

The determination of the lateral amplification, linearity and perpendicularity characteristics requires a calibrated material measure in the form of a two-dimensional (2D) cross-grating [4]. The cross-grating can be used to establish the scales of the  $x$ - and  $y$ -axes. FVM cannot measure commonly available cross-gratings that are smooth. Therefore, a new cross-grating artefact that can be measured with FVM needs to be designed and manufactured to calibrate the lateral performance.

The proposed cross-grating artefact has hemispherical groove features (called ‘calottes’ from now onwards) produced by a Kern Evo high-precision micro-milling machine from a block of stainless steel (grade 303). The artefact design is a square block of size of 28 mm with 5 mm thickness, and contains 36 calottes with nominal diameters of 0.5 mm. The nominal distance between two calottes is 4 mm.

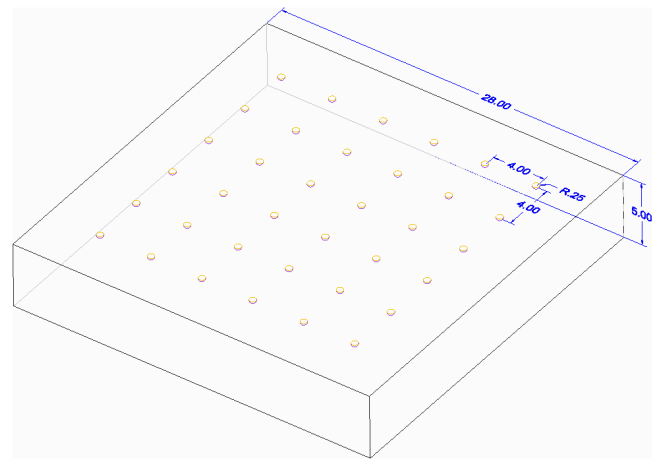


Figure 1. The artefact design.

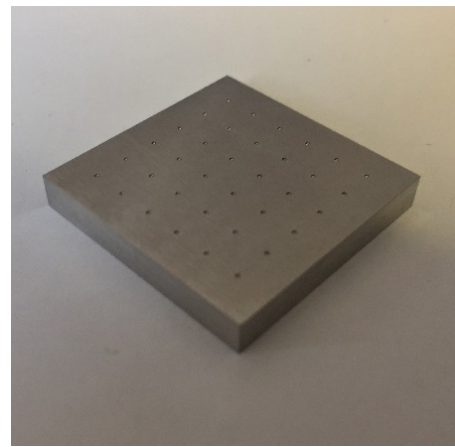


Figure 2. The manufactured artefact.

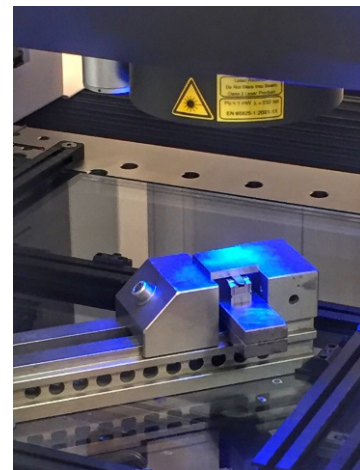


Figure 3. The artefact calibration with the CMM.

The artefact is designed to capture the scale error of the  $xy$ -stage for measurements both with and without stitching, and is presented in figure 1, which shows the nominal length and thickness of the artefact. The 36 calottes are in the form of a  $6 \times 6$  grid. The total area of the grid is  $24 \times 24$  mm. This selection is based on common multiple image-field measurements that are usually within an area from  $3 \times 3$  mm to  $15 \times 15$  mm.

**Table 1.** All influence factors of the calibration process. The calculation for the largest uncertainty among all the centre distances is shown.

Sources	Value/ $\mu\text{m}$	Description
$u_{\text{rep}}$	0.817	Influence factor considering the CMM repeatability, part property (form, texture), sampling strategy, contamination of the surface, etc (Type A)
$u_{\text{geo}}$	0.316	Influence factor considering CMM geometric error, stylus error, tip error, fixturing error and alignment error (Type A)
$u_{\text{corr}}$	0.052	Influence factor considering the length error correction applied to the length measurement (only applied for distance/length and size measurement) (Type B)
$u_{\text{temp}}$	0.005	Influence factor due to thermal variation and error of coefficient thermal expansion of the measured part (Type B)
$u_{\text{gaugeblock}}$	0.045	Influence factor from the measurement of the calibrated gauge block (Grade 1 gauge block) (Type B)
$u_{\text{total}}$	0.88	Combined standard uncertainty

Firstly, a face milling process, using a 6 mm diameter carbide end mill, was applied to flatten the top surface of the block. The spindle speed and the feedrate of the face milling process were 5000 rpm and  $300 \text{ mm min}^{-1}$ , respectively. Secondly, the calotte features were machined by a 0.5 mm diameter carbide ball nose mill with the same spindle speed and a feedrate. The final surface texture for the top face of the artefact was achieved with a lapping process using a Kemet LM15 lapping machine. The artefact was made of stainless steel to create a surface with texture that complies with the FVM requirement. Figure 2 shows the manufactured cross-grating artefact. The  $Sa$  of the manufactured artefact is  $(0.357 \pm 0.004) \mu\text{m}$  using nesting indices of  $S$ -filter =  $2.5 \mu\text{m}$  and  $L$ -filter =  $250 \mu\text{m}$ .

## 2.2. Calibration of the material measures

In order to calibrate the distances between the centres of the calottes of the cross-grating, a Zeiss O-Inspect non-contact coordinate measuring machine (CMM) was used with a maximum permissible error specification of  $E_{L,\text{MPE}} = \pm (1.6 + L/300) \mu\text{m}$ , where  $L$  is in mm. This CMM is periodically performance verified to assure that it operates within its specification  $E_{L,\text{MPE}}$ . According to the specification, the CMM has one-magnitude higher accuracy for its  $x$ - and  $y$ -stages compared to that of the FVM, so that the distances between the centre of the calottes measured by the CMM can be used as the length reference, that is traceable via a gauge block measurement, for the distances measured by FVM. The calottes' centre measurements were carried out in four different positions with different orientations at each position. The orientation is changed by rotating the artefact by  $90^\circ$  clock-wise for each position. Measurements were repeated five times for each calotte at each position. With this strategy (ISO/TS 15530-2) [16], the volumetric error of the CMM is taken into account as a contributor for the combined standard uncertainty estimation of the artefact's measurement results. Figure 3 shows the artefact calibration with the CMM, where one of the four artefact calibration positions is shown. The artefact position is not parallel to the CMM's  $x$ - and  $y$ -axes (skewed position) so that the CMM will move both the  $x$ - and  $y$ -axes to reach each calotte. By moving both axes, the errors from both axes are taken into account as influence factors in the uncertainty estimation of the calottes' centre measurements. The calottes' centre measurements were carried

out by the CMM optical-head with a 2D vision system. For the traceability, the measurement of a calibrated gauge block was carried out by using the tactile sensor of the CMM.

The location of the centre of each calotte was measured and the centre distances between pairs of calottes were calculated. The centre locations are obtained by an image processing algorithm that extracts the points of the detected circle of calottes and associates a circle geometry to the extracted points to obtain the centre location of the calottes. Table 1 shows details of the uncertainty estimation for the centre distance and maximum combined uncertainty of a distance between two calottes on the artefact. In table 1, all influence factors are detailed. The factors consider the CMM repeatability, CMM geometric error, temperature variation and uncertainty for the length measurement of a Grade 1 gauge block. The measurement uncertainty of the length (the centre distance between two calottes) was estimated according to ISO/DTS 15530-2 for calibration with a CMM [16]. Traceability of the calibration results is established with a substitution measurement of the gauge block, with the tactile sensor of the CMM, with nominal length 4 mm (equal to the nominal length being calibrated).

## 2.3. Experimental design

Two objective lenses of  $5\times$  and  $10\times$  magnifications have been chosen to measure the cross-grating artefact in  $x$ -(horizontal),  $y$ -(vertical) and diagonal directions. The image fields of the  $5\times$  and  $10\times$  objectives are  $2.82 \times 2.82 \text{ mm}$  and  $1.62 \times 1.62 \text{ mm}$ , respectively. The objectives have been chosen to give a relatively large size of image field. The area of measurements are larger than the image field of both the objectives. The measurements are carried out at one height ( $z$ -direction) location (at the height of the instrument table where parts are placed) as the calibration is focused on the lateral performance of the FVM. Four measurement types have been determined: measurement in horizontal, vertical and diagonal directions (see figure 4), and measurements for the whole calottes grid. Each measurement type is replicated three times and averaged to reduce random error. Both stitching and non-stitching measurement methods are applied. With stitching, the surfaces in between two calottes are measured, and with non-stitching only the calottes' centres are determined, without measuring the surfaces in between.

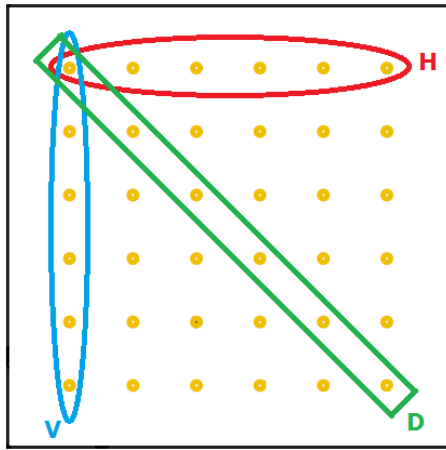


**Figure 4.** Horizontal (H), vertical (V) and diagonal (D) directions of the measurements.

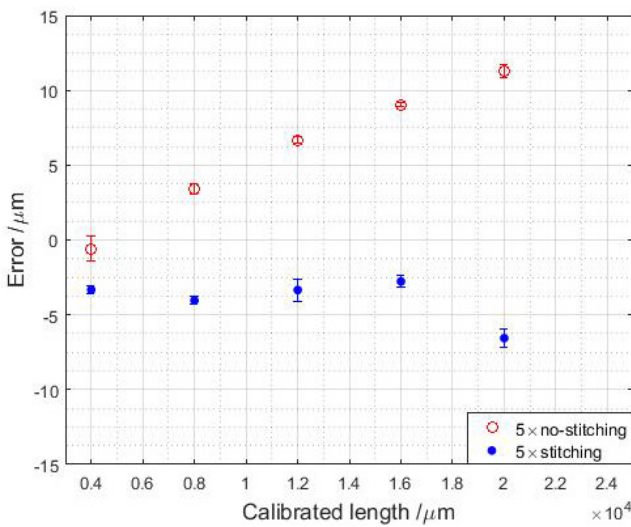


**Figure 5.** Results of the error calculation for the 5× objective in the horizontal direction.

The purpose of investigating the stitching measurements is to study the effect of the stitching algorithm with respect to the lateral stage accuracy. The stitching measurements involve the measurement of multiple image-fields that overlap with each other and the point registration of the overlapped image-fields to reduce the error of the lateral stage. The measurements from the horizontal and vertical directions are used to calculate the perpendicularity error. For amplification and linearity in 2D, all the calottes are measured only with a stitching method, with both 5× and 10× objective lens magnifications, and 2D error maps are presented.

### 3. Lateral scale calibration results

#### 3.1. Amplification and linearity deviation

The amplification and linearity of the  $xy$ -stage are determined by calculating the errors between two calottes' centres from measurements in the  $x$ -,  $y$ - and diagonal directions. The calotte centres are calculated as the centre of a sphere associated to the 3D point cloud of the calottes. An error is defined as the

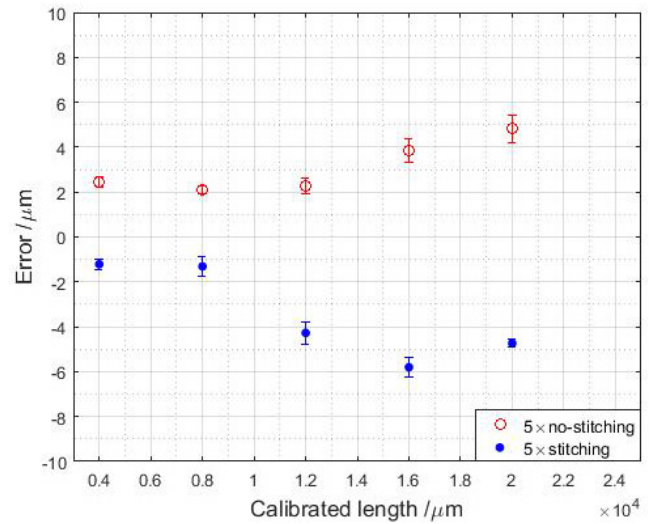


**Figure 6.** Results of the error calculation for the 5× objective in the vertical direction.

difference between a calibrated length (measured by CMM) and a length measured by FVM. The length is the distance between two calottes' centres. The results show different errors for the measurements carried out in different measuring directions with both the objectives 5× and 10× and with and without stitching. In addition, the results show that the choice of the different objective lenses does not significantly affect the error, but the use of stitching does have a significant effect.

Figures 5–7 show the errors of the length measurements with the 5× objective lens for the horizontal, vertical and diagonal directions respectively. From figures 5 and 6, it can be seen that the average length errors measured with stitching are reduced by up to 52% and 25% for the  $x$ - and  $y$ -directions respectively, compared to the errors obtained from the measurements without stitching. Similarly, figures 8–10 show the errors for the measurements with the 10× objective lens for horizontal, vertical and diagonal directions respectively. From figures 8 and 9, the average length errors can be reduced by up to 62%, and 10%, for  $x$ - and  $y$ -directions respectively, for measurement with stitching compared to without stitching. The length errors in the diagonal direction obtained from both the 5× and 10× objective lenses are similar for both stitching and non-stitching measurement strategies. The results show that the stitching algorithm is only effective for measurement in the single  $x$ - and  $y$ -directions, but is not as effective in the diagonal direction.

From the non-stitching measurements with both the 5× and 10× objective lenses, the results show that the lateral error of the stage is the largest in the  $x$ -direction. Since the non-stitching strategy measures each calotte separately to calculate their centre positions, their errors cannot be numerically compensated. Numerical compensations are applied by stitching overlapping surfaces when the calottes are measured. The measurement results obtained by the 10× objective lens with the stitching method have lower errors than the measurements obtained by the 5× objective lens. Larger numbers of images for stitching are obtained to reconstruct the measured surfaces with the 10× objective lens due to a smaller field

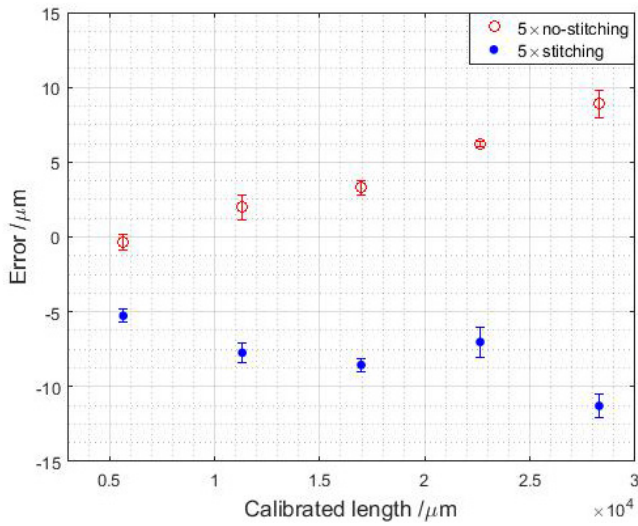


Figure 7. Results of the error calculation for the 5× objective in the diagonal direction.

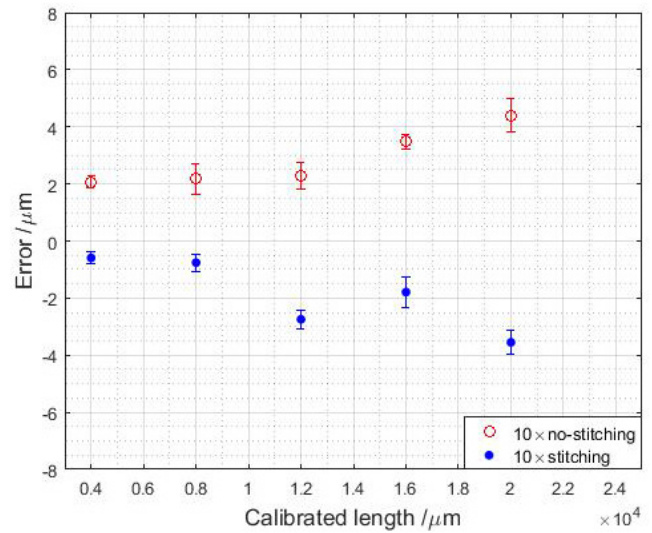


Figure 9. Results of the error calculation for the 10× objective in the vertical direction.

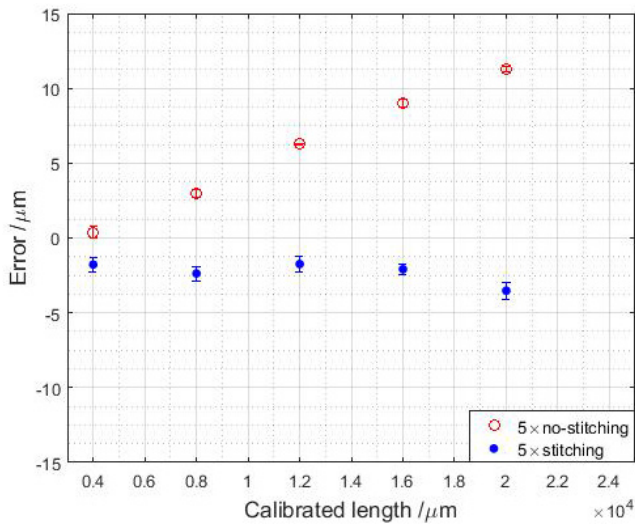


Figure 8. Results of the error calculation for the 10× objective in the horizontal direction.

of view. Subsequently, with larger numbers of images for stitching, compensation of the stage’s error can be improved so that the measurement error is reduced. The higher error of the non-stitching method may be due to the backlash of the  $xy$ -stage screw thread. The errors from non-stitching measurement increase linearly proportional to the measured length, which is typical for the backlash of a linear stage [17].

The measurement uncertainty of length errors considers several influence factors: the standard error from measurement repetitions, the uncertainty of the length calibration, the error due to the material expansion and the error in the estimation of the coefficient of the material’s thermal expansion coefficient. Table 2 shows the influence factors that contribute to the measurement uncertainty. In table 2, the largest uncertainty estimation corresponding to a 20 mm length measurement is shown. The combined standard uncertainty for the 20 mm length measurement is 1.48  $\mu\text{m}$ .

According to the results of an analysis of variance (ANOVA), the length measurement errors obtained with the 5× and 10× objectives are statistically similar for all the measurements in  $x$ -,  $y$ - and diagonal-directions. The results show that the errors are mostly contributed by the performance of the  $xy$ -stage. Therefore, changing the objective may not significantly affect the results of the calibration. Giusca et al [6] also reported that errors of amplification, linearity and perpendicularity of the  $xy$ -stage of other instruments are not affected by the magnification of the objectives. The results suggest that a low magnification lens can be used to determine the amplification and linearity errors of the  $xy$ -stage. By using a low magnification lens, a larger field of view can be obtained so that measurement time can be reduced.

In summary, the results of the amplification coefficient ( $\alpha$ ) and linearity deviation ( $l$ ), following their definition in ISO/DIS 25178 [2], are numerically presented in table 3. From table 3, the calculated amplification coefficients show that the measurements with stitching tend to decrease the measured distance and the measurements without stitching tend to increase the measured distance between the centres of two callottes. The amplification coefficients calculated from the measurements with stitching have value less than one unity, meaning the measured distances are shorter than the calibrated distances. In contrast, the coefficients calculated from measurements without stitching have values more than unity, meaning the measured distances are longer than the calibrated distances. From the calculated linearity deviation shown in table 3, the results show that, even though the measurements with stitching decrease the stage errors, they also increase the non-linearity. It is worth noting that the stage error and linearity deviation are different. The stage errors show the difference between a measured and calibrated distance between two callottes’ centres, while linearity deviations show the maximum difference between the measured data and the line from which the amplification coefficient is derived [2].

**Table 2.** Measurement uncertainty estimation and its influence factors. The shown estimated combined uncertainty is the largest uncertainty estimation among the errors measured with the 5× and 10× objective lenses corresponding to a 20 mm length measurement.

Uncertainty contributor	Value/ $\mu\text{m}$	Description
$u_{\text{rep}}$	1.17	Standard error from multiple measurements (Type A)
$u_{\text{temp}}$	0.23	Uncertainty due to stainless steel coefficient of thermal expansion (CTE) $11.7 \times 10^{-6} \text{ K}^{-1}$ and $\Delta T = 1 \text{ }^\circ\text{C}$ (Type B)
$u_{\text{CTE}}$	0.023	Uncertainty due to error in the CTE estimation (10% CTE) (Type B)
$u_{\text{trace}}$	0.88	Uncertainty of calibration of the length (Type B)
$u_{\text{total}}$	1.48	Combined uncertainty

**Table 3.** The calculated values of amplification coefficient and linearity deviation.

Amplification coefficient ( $\alpha$ )	5×		10×	
	Stitching	Non-stitching	Stitching	Non-stitching
$\alpha_x$	0.99987	1.0007	0.99992	1.00069
$\alpha_y$	0.99971	1.00016	0.99982	1.00015
$\alpha_{\text{diagonal}}$	0.9998	1.0004	0.99983	1.00045
Linearity deviation ( $l$ )	Stitching	Non-stitching	Stitching	Non-stitching
$l_x/\mu\text{m}$	1.24	0.51	0.41	0.21
$l_y/\mu\text{m}$	0.84	0.60	0.61	0.42
$l_{\text{diagonal}}/\mu\text{m}$	1.47	0.51	0.51	0.73

**Table 4.** Results of perpendicularity deviation ( $\pm$ standard deviation of the mean).

	5× stitching/ $^\circ$	5× non-stitching/ $^\circ$	10× stitching/ $^\circ$	10× non-stitching/ $^\circ$
FVM	$90.46 \pm 0.53$	$89.77 \pm 0.20$	$90.22 \pm 0.07$	$90.19 \pm 0.46$
CMM			$89.99 \pm 0.01$	
Difference	0.46	0.22	0.22	0.19

### 3.2. Perpendicularity deviation

The perpendicularity deviation is obtained by calculating the differences of the angles between the  $x$ - and  $y$ -axes from the CMM measured data and from the FVM measured data. For the perpendicularity deviation, the calottes' centre locations are estimated from the measurements in the  $x$ - and  $y$ -directions, using stitching and non-stitching strategies. Three repeated measurements are carried out for stitching and non-stitching measurements to estimate the calottes' centre locations. From the estimated calottes' centre locations, least-square lines are fitted to the centre locations in both the  $x$ - and  $y$ -directions. The perpendicularity deviation the 5× and 10× objective lenses are  $0.46^\circ$  and  $0.22^\circ$  for the measurements with stitching, and  $0.22^\circ$  and  $0.19^\circ$  for the measurements without stitching, respectively. Table 4 shows the results of all perpendicularity deviations. From table 4, the maximum differences for the perpendicularity deviation for both stitching and non-stitching measuring strategies, and both the objective lenses are around  $\pm 0.2^\circ$ . Giusca *et al* [6] also found a similar perpendicularity deviation of  $0.3^\circ$  with a coherence scanning interferometer.

### 3.3. Amplification and linearity errors in 2D

The amplification and linearity deviation in  $xy$ -directions are presented as 2D error maps. The 2D error maps for measurements with the 5× and 10× objectives lenses are shown in

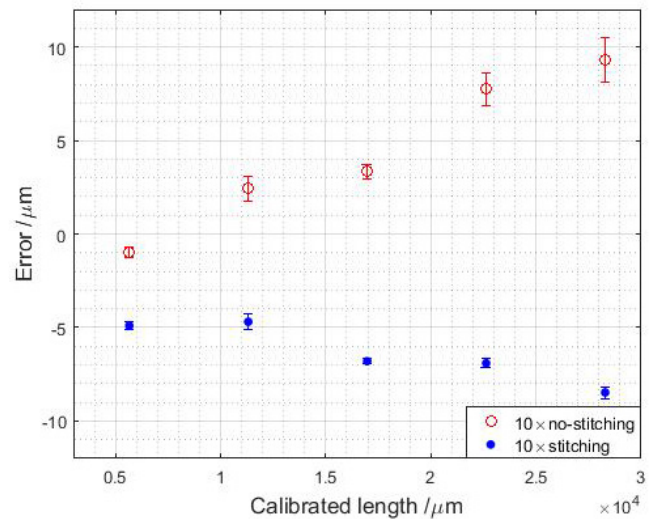


**Figure 10.** Results of the error calculation for the 10× objective in the diagonal direction.

figures 11 and 12 respectively. For all the measurements, stitching is employed and the measurements cover the whole surface of the artefact. All the calottes' centre locations are calculated from the average of three repeated measurements. The coordinates of the calculated centres are mathematically aligned, by least-squares fitting a line to the calottes' central position, calculating the angle of the fitted line with respect to the  $x$ -axis of the reference coordinate system and

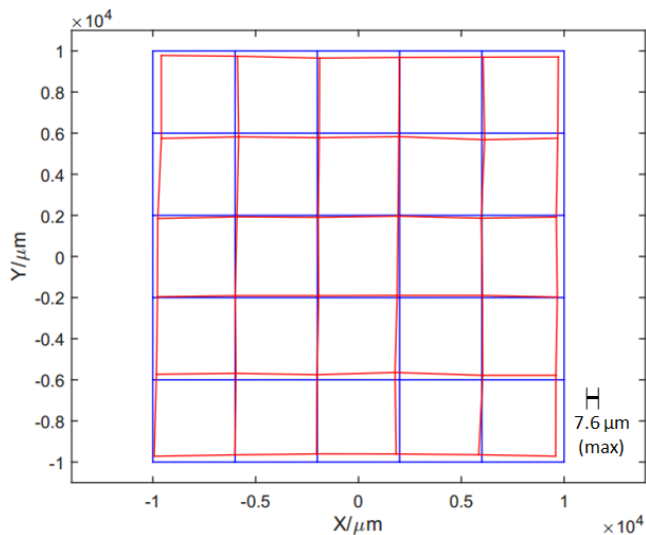


**Figure 11.** 2D error map for the measurement obtained with the 5× objective lens (the FVM data is red and the CMM is blue).

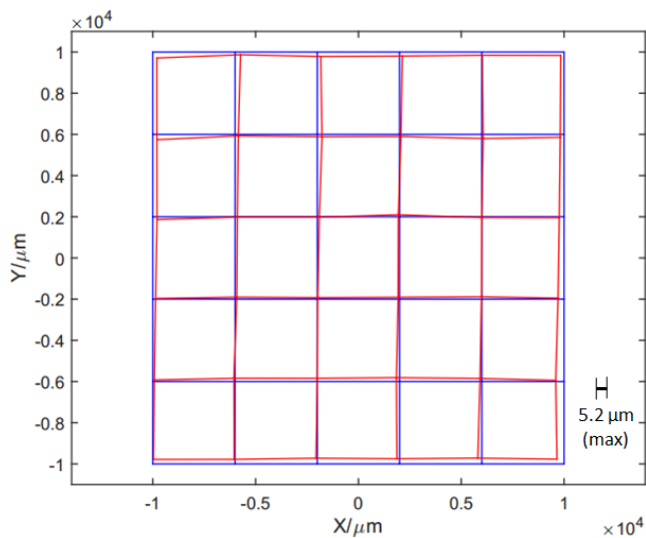


**Figure 12.** 2D error map for the measurement obtained with the 10× objective lens (the FVM data is red and the CMM is blue).

rotating all the central positions based on the calculated angle, to remove errors due to fixturing and placement when setting up the artefact for the measurements. After the alignment, all centre locations from both the measurements of CMM and FVM are registered and overlapped, by translating the coordinate system of all the centre positions (from both the CMM and FVM measurements) to the centroid position of the centre location, based on their centroid locations [18]. After all the centre locations have been registered and overlapped, the errors of each centre's location on the grid are calculated as the difference between the centre locations measured with the FVM and centre locations measured with the CMM. The centre locations measured with the CMM are used as reference values. The maximum differences between the CMM and FVM measurements with the 5× and 10× objective lenses are 7.6 μm and 5.2 μm, respectively.

From the 2D error maps, it can be seen that the measurement errors with stitching, for both the 5× and 10× objectives

lenses, are generally 15% higher than the errors in the single axis measurements with stitching. The increase of the errors can be attributed to the contribution of both the  $x$ - and  $y$ -axis errors for the 2D measurements.

#### 4. Conclusion and future work

This paper presents the calibration of the lateral scale for FVM by determining its amplification, linearity and perpendicularity characteristics. A novel and low-cost calibrated cross-grating artefact, consisting of a grid of calottes, and procedures for the determination of linearity, amplification and perpendicularity characteristics have been proposed. As part of this study for determining the characteristics, two objective lenses of 5× and 10× were used to measure the proposed cross-grating artefact with both stitching and non-stitching strategies. Measurements in the horizontal, vertical and diagonal directions, along with measurements of the entire grid of calottes, were carried out. The results from the measurements of the proposed cross-grating artefact indicate that:

1. Measurements with stitching can reduce errors in the  $x$ - and  $y$ -directions, but not in the diagonal direction.
2. Measurements in 2D direction has 15% larger errors than measurements in only one direction.
3. Measurements with stitching can significantly reduce lateral stage error, but increase the non-linearity of the error.

Future research will include designing and manufacturing a cross-grating artefact that can be measured within one image field so that amplification, linearity and perpendicularity characteristics can be determined while excluding lateral stage errors. Further work will investigate how to determine the remaining metrological characteristics for FVM, i.e. the topographic spatial resolution and topography fidelity.

#### Acknowledgments

This work was supported by the Engineering and Physical Sciences Research Council (grant number EP/M008983/1) and King Abdulaziz City for Science and Technology (KACST) of the Saudi Government.

#### ORCID iDs

Wahyudin P Syam  <https://orcid.org/0000-0002-4553-9611>

#### References

- [1] Leach R K 2011 *Optical Measurement of Surface Topography* (Berlin: Springer)
- [2] ISO/DIS 25178: 600 2017 *Geometrical product specifications (GPS)—Surface Texture: Areal—Part 600: Metrological Characteristics for Areal-Topography Measuring Methods* (International Organisation for Standardization)
- [3] Leach R K, Giusca C L, Haitjema H, Evans C and Jiang X 2015 Calibration and verification of areal surface texture measuring instruments *Ann. CIRP* **64** 797–813

- [4] ISO 25178-6 2010 *Geometrical Product Specifications (GPS)—Surface Texture: Areal—Part 6: Classification of Methods for Measuring Surface Texture* (International Organisation for Standardization)
- [5] Giusca C L, Leach R K, Helary F, Gutauskas T and Nimishakavi L 2012 Calibration of the scales of areal surface topography-measuring instruments: part 1. Measurement noise and residual flatness *Meas. Sci. Technol.* **23** 035008
- [6] Giusca C L, Leach R K and Helery F 2012 Calibration of the scales of areal surface topography measuring instruments: part 2. Amplification, linearity and squareness *Meas. Sci. Technol.* **23** 065005
- [7] Giusca C and Leach R K 2013 Calibration of the scales of areal surface topography measuring instruments: part 3. Resolution *Meas. Sci. Technol.* **24** 105010
- [8] Leach R K 2014 *Fundamental Principles of Engineering Nanometrology* 2nd edn (Amsterdam: Elsevier)
- [9] Hiersemenzel F, Petzing J, Leach R K, Helmlı F and Singh J 2012 Areal texture and angle measurements of tilted surfaces using focus variation methods *Proc. 3rd Int. Conf. Surface Metrology (Annecy, France, 21–23 March)*
- [10] Danzl R, Helmlı F and Scherer S 2009 Focus variation—a new technology for high resolution optical 3D surface metrology *Proc. 10th Int. Conf. Slovenian Society for Non-Destructive Testing ‘Application of Contemporary Non-Destructive Testing in Engineering’ (Ljubljana, Slovenia, 1–3 September)* pp 481–91
- [11] Danzl R, Helmlı F and Scherer S 2011 Focus variation—a robust technology for high resolution optical 3D surface metrology *Stroj. Vestn. J. Mech. Eng.* **57** 245–56
- [12] Moroni G, Syam W P and Petró S 2018 A simulation method to estimate task-specific uncertainty in 3D microscopy *Measurement* **122** 402–16
- [13] Macdonald D 2014 The application of focus variation microscopy for lithic use-wear quantification *J. Archaeol. Sci.* **48** 26–33
- [14] ISO/DIS 25178: 700 2016 *Geometrical Product Specifications (GPS)—Surface Texture: Areal—Part 700: Calibration and Verification of Areal Topography Measuring Instruments* (Geneva: International Organization for Standardisation)
- [15] Giusca C L, Claverley J, Sun W, Leach R K, Helmlı F and Chavigner M 2014 Practical estimation of measurement noise and flatness deviation on focus variation microscopes *Ann. CIRP* **63** 545–8
- [16] ISO/DTS 15530-2 2007 *Geometrical Product Specifications (GPS)—Coordinate Measuring Machines (CMM): Technique for Determining the Uncertainty of Measurement—Part 2: Use of Multiple Measurement Strategies* (International Organization for Standardisation)
- [17] Smith S T 2018 *Precision machine principles and elements Basics of precision Engineering* ed R K Leach and S T Smith (Boca Raton, FL: CRC Press)
- [18] Daemi B, Ekberg P and Mattsson L 2017 Lateral performance evaluation of laser micromachining by high precision optical metrology and image analysis *Precis. Eng.* **50** 8–19